Heme Oxidation in a Chimeric Protein of the α-Selective *Neisseriae meningitidis* Heme Oxygenase with the Distal Helix of the δ-Selective *Pseudomonas aeruginosa*†

Rahul Deshmukh,‡,§ Yuhong Zeng,|| Lena M. Furci,‡ Hong-wei Huang,⊥ Bailey N. Morgan,|| Suzanne Sander,|| Aileen Y. Alontaga,|| Richard A. Bunce,@ Pierre Moënne-Loccoz,⊥ Mario Rivera,*,|| and Angela Wilks*,‡

Department of Environmental and Biomolecular Systems, OGI School of Science and Engineering at Oregon Health and Science University, Beaverton, Oregon 97006-8921, Department of Chemistry, The University of Kansas, 1251 Wescoe Hall Drive, Lawrence, Kansas 66045-7582, Department of Chemistry, Oklahoma State University, Stillwater, Oklahoma 74078-3071, and Department of Pharmaceutical Sciences, School of Pharmacy, University of Maryland, Baltimore, Maryland 21201-1180

Received May 2, 2005; Revised Manuscript Received August 11, 2005

ABSTRACT: Heme oxygenases from the bacterial pathogens *Neisseriae meningitidis* (*nm*-HO) and *Pseudomonas aeruginosa* (*pa*-HO) share significant sequence identity (37%). In *nm*-HO, biliverdin IXα is the sole product of the reaction, whereas *pa*-HO yields predominantly biliverdin IXδ. We have previously shown by NMR that the in-plane conformation of the heme in *pa*-HO is significantly different from that of *nm*-HO as a result of distinct interactions of the heme propionates with the protein scaffold [Caignan, G. A., Deshmukh, R., Wilks, A., Zeng, Y., Huang, H. W., Moenne-Loccoz, P., Bunce, R. A., Eastman, M. A., and Rivera, M. (2002) *J. Am. Chem. Soc. 124*, 14879−14892]. In the report presented here, we have extended these studies to investigate the role of the distal helix by preparing a chimera of *nm*-HO (*nm*-HOch), in which distal helix residues 107−142 of *nm*-HO have been replaced with the corresponding residues of the δ-regioselective *pa*-HO (112−147). Electronic absorption spectra, resonance Raman and FTIR spectroscopic studies confirm that the orientation and hydrogen bonding properties of the proximal His ligand are not significantly altered in the chimera relative those of the wild-type proteins. The catalytic turnover of the *nm*-HOch-heme complex yields almost exclusively α-biliverdin and a small but reproducible amount of δ-biliverdin. NMR spectroscopic studies reveal that the altered regioselectivity in the chimeric protein likely stems from a dynamic equilibrium between two alternate in-plane conformations of the heme (in-plane heme disorder). Replacement of K16 with Ala and Met31 with Lys in the chimeric protein in an effort to tune key polypeptide−heme propionate contacts largely stabilizes the in-plane conformer conducive to δ-meso hydroxylation.

Until the recent characterization of the *Pseudomonas aeruginosa* heme oxygenase (*pa*-HO)[1] (*1*), all known heme oxygenases, including those from *Neisseriae meningitidis* (*nm*-HO) and *Corynebacterium diphtheriae* (*cd*-HO) were shown to specifically cleave the heme at the α-meso carbon (*2*, *3*). In addition, the crystal structures of the mammalian heme oxygenases (*4*−*8*) and the bacterial *nm*-HO (*9*−*11*) clearly identify a role for the distal helix in sterically restricting access to all but the α-meso carbon. Interestingly, the level of sequence identity (less than 15%) between *nm*-HO and the mammalian enzymes is extremely low, yet the same overall structural fold is observed in both proteins (*4*, *10*). In contrast, the level of sequence identity (37%) between the α-selective *nm*-HO and δ-selective *pa*-HO is significantly higher, suggesting a similar overall fold in keeping with the previous structurally characterized HO proteins. Our previous ^{1}H NMR studies have shown that in contrast to *nm*-HO and all α-selective heme oxygenases the heme environment in *pa*-HO is significantly different (*12*). The NMR data indicated an approximately 110° in-plane rotation of the heme in *pa*-HO relative to other known bacterial and mammalian HOs, which are all exclusively α-regioselective (*12*). Analysis of the crystal structure of *nm*-HO revealed the conserved Lys-16 and Tyr-112 residues (Figure 1B), which are positioned to interact with the heme propionates and aid in binding and orienting the heme for α-regioselective oxidation (*10*). Amino acid sequence comparisons in the context of the structure of *nm*-HO suggested the absence of these conserved residues in *pa*-HO. Lys-16

† This work was supported by NIH Grants AI55912 (A.W.) and GM50503 (M.R.).

* To whom correspondence should be addressed. A.W.: fax, (410) 706-5017; e-mail, awilks@rx.umaryland.edu. M.R.: fax, (785) 864-5936; e-mail, mrivera@ku.edu.

‡ University of Maryland.

§ Current address: Department of Basic Pharmaceutical Sciences, School of Pharmacy, West Virginia University, Morgantown, WV 26506-9530.

|| The University of Kansas.

⊥ OGI School of Science & Engineering at Oregon Health and Science University.

@ Oklahoma State University.

[1] Abbreviations: heme, iron protoporphyrin IX regardless of oxidation and ligation state; hHO-1, human heme oxygenase; *nm*-HO, *N. meningitidis* heme oxygenase; *pa*-HO, *P. aeruginosa* heme oxygenase; *cd*-HO, *C. diphtheriae* heme oxygenase; HO, heme oxygenase; FTIR, Fourier transform infrared; NMR, nuclear magnetic resonance; RR, resonance Raman.

10.1021/bi050810t CCC: $30.25 © 2005 American Chemical Society
Published on Web 09/29/2005

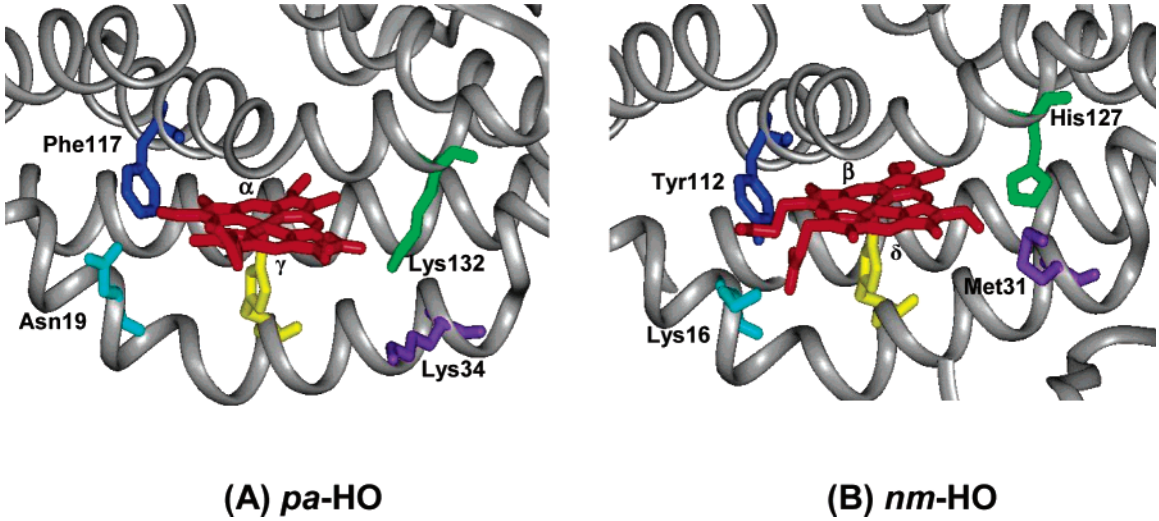

FIGURE 1: Crystal structures of *pa*-HO (A) and *nm*-HO (B) showing the locations of some key amino acid residues in the heme binding site, which control the regioselectivity through the interactions between their side chains and heme propionates. The orientations of the heme in the two enzymes are related to each other by an 80° in-plane rotation. The crystal structures of *pa*-HO and *nm*-HO are Protein Data Bank entries 1SK7 and 1J77, respectively.

and Tyr-112 being replaced with Asn-19 and Phe-117, respectively, suggested that the absence of favorable interactions with the heme propionate may result in the ~110° in-plane rotation of the heme in *pa*-HO relative to α-biliverdin-producing HOs (Figure 1A). When Asn-19 and Phe-117 in *pa*-HO were replaced with Lys and Tyr, respectively, to introduce interactions with heme propionates characteristic of α-biliverdin-forming enzymes (see Figure 1B), ^{1}H and ^{13}C NMR studies revealed that the heme in the *pa*-HO N19K/F117Y double mutant exists in a dynamic equilibrium between two in-plane conformations (seatings). One of these seatings is identical to wild-type *pa*-HO, and the other is more typical of the α-regioselective heme oxygenases (*12*). This dynamic exchange, which amounts to a 110° in-plane rotation of the heme between two seatings, profoundly affects the regioselectivity of heme oxidation, as evidenced by the formation of α-biliverdin (55%), *δ*-biliverdin (35%), and *β*-biliverdin (10%) (*12*).

The recently determined crystal structure of *pa*-HO (*13*) (Figure 1A) confirmed that the heme in *pa*-HO is indeed rotated in-plane by ~110° relative to that of the α-hydroxylating heme oxygenases. The crystal structure of *pa*-HO also suggests that Lys-34 and Lys-132 are within hydrogen bonding distance of the heme propionate (Figure 1A), and a recent study has shown that ~12% α-biliverdin is formed when Lys-34 or Lys-132 is mutated to Ala (*14*).

We have recently carried out an in-depth analysis of the Arg-177 Glu and Asp mutants in *cd*-HO in which the formation of *δ*-biliverdin, again, is a direct consequence of an in-plane rotation of the heme triggered by electrostatic repulsion between the heme propionate and the protein scaffold upon replacement of the positively charged side chain of Arg-177 with a negatively charged Glu or Asp residue (*15*). The introduction of electrostatic repulsion between the heme propionate and Glu-177 results in an 85° in-plane rotation of the heme such that the *δ*-meso carbon is placed at the position equivalent to that occupied by the α-meso carbon within the wild-type *cd*-HO protein fold, thus rendering the *δ*-meso carbon susceptible to hydroxylation (*15*).

Herein, we report that replacement of the distal helix of the α-selective *nm*-HO, residues 107−142, with those of the *δ*-selective *pa*-HO, residues 112−147, did not significantly alter the regioselectivity of the reaction. The chimeric protein oxidizes heme to produce ~95% biliverdin IXα and ~5% biliverdin IX*δ*. Characterization of the chimeric protein by UV−visible and resonance Raman spectroscopy suggests a well-organized protein with distal pocket properties similar to those of *pa*-HO. NMR spectroscopy, on the other hand, reveals in-plane heme disorder that accounts for the formation of biliverdin IX*δ*.

EXPERIMENTAL PROCEDURES

General Methods. Plasmid purification, subcloning, and bacterial transformations were carried out as previously described (*16*). Deionized, doubly distilled water was used for all experiments. Oligonucleotides were obtained from Sigma-Genosys and used without further purification. All absorption spectra of the heme−HO complexes were recorded on a Cary Varian Bio100 UV spectrophotometer.

Bacterial Strains. Escherichia coli strain DH 5α [F′, *ara* D(*lac-proAB*) rpsL ø80d*lacZ*DM15 *hsd* R17] was used for DNA manipulation, and *E. coli* strain BL21(DE3) *pLysS* [F^{-} *ompT hsdS*$_{B}$ ($r_{B}^{-}m_{B}^{-}$) *gal dcm* (DE3)] was used for expression of both the wild-type and mutant heme oxygenase constructs.

Site-Directed Mutagenesis of nm-HO. Mutagenesis was carried out utilizing the polymerase chain reaction and the Quickchange mutagenesis kit from Stratagene (La Jolla, CA). Oligonucleotides were designed to have melting temperatures (T_m) between 65 and 75 °C. All mutations were verified by DNA sequencing of the gene construct. DNA sequencing was carried out at the Biopolymer Laboratory, School of Medicine, University of Maryland. The *nm*-HOch construct was engineered by introducing an *Avr*II restriction site into the DNA sequence corresponding to amino acids ^{107}AIGWL^{111} and ^{112}ALGWL^{116} and a *Sac*I site in the sequence corresponding to residues ^{138}GARHL^{142} and ^{143}GARHL^{147} in *nm*-HO and *pa*-HO, respectively. Following confirmation of the sites by restriction digest and sequencing,

the distal helix of *pa*-HO was excised and subcloned into *nm*-HO utilizing the introduced *Sac*I and *Avr*II sites. The *nm*-HO mutant constructs were verified by restriction digest and confirmed by DNA sequencing.

Expression and Purification of the Wild Type and nm-HO Mutants. The wild-type and mutant *nm*-HO proteins were purified as previously described (*1*, *2*). A single colony of freshly transformed *E. coli* BL21(DE3) *plysS* cells was cultured overnight in 5 mL of LB medium containing 100 μg/mL ampicillin. The cells were subsequently subcultured into fresh LB−ampicillin medium (100 mL) and grown at 37 °C to mid-log phase. The cells were then subcultured (10 mL) into LB−ampicillin medium (1 L) and on reaching mid-log phase expression were induced by addition of isopropyl 1-thiol-D-galactopyranoside (IPTG) to a final concentration of 1 mM. The cells were grown further for 4−5 h at 30 °C and harvested by centrifugation (10000*g* for 20 min). Cells were lysed by sonication in 50 mM Tris-HCl (pH 7.8) containing 1 mM EDTA and 1 mM phenylmethanesulfonyl fluoride (PMSF). The cell suspension was then centrifuged at 27000*g* for 40 min.

The soluble fraction was applied to a Sepharose-Q Fast Flow column (1.5 cm × 10 cm) previously equilibrated with 20 mM Tris-HCl (pH 7.5). The column was washed with 3 volumes of 20 mM Tris-HCl (pH 7.5) containing 50 mM NaCl. The protein was then eluted with the same buffer with a linear gradient of NaCl from 50 to 500 mM. The protein eluted at a concentration of 150 mM NaCl, and the peak fractions were pooled and dialyzed against 10 mM potassium phosphate (pH 7.4) (2 × 4 L) at 4 °C. The protein was then stored at −80 °C or reconstituted with heme as described below.

Reconstitution of the Wild-Type and Mutant nm-HO Proteins with Heme. The heme−*nm*-HO complexes were prepared as described previously (*17*, *18*). Hemin was added to the purified HO proteins at a final 2:1 heme:protein ratio. The sample was then passed over a Sephacryl S-100 HR column (3.0 cm × 100 cm) pre-equilibrated with 20 mM Tris-HCl (pH 7.8). The protein was then eluted with 20 mM Tris (pH 7.8), and the fractions containing the purified protein were pooled and dialyzed (2 × 4 L) against 20 mM Tris-HCl (pH 7.8) at 4 °C. The protein was concentrated by an Amicon filtration unit and stored at −80 °C. Samples for NMR and resonance Raman analysis were passed down an additional Sephacryl S-100 HR column (3.0 cm × 100 cm) following concentration on an Amicon filtration unit.

Absorption Spectroscopy of the nm-HO Wild-Type and Mutant Proteins. The UV−visible spectra of the wild-type HOs and their respective mutants were recorded in 20 mM Tris (pH 7.5) on a Cary 100Bio spectrophotometer. The Fe^{II}−CO spectra were obtained by saturating the solution with CO followed by the addition of a few grains of sodium dithionite. The $Fe^{II}-O_2$ complexes were obtained by passage of the Fe^{II}−CO complexes through a Sephadex G-25 column (1 cm × 3 cm). The millimolar extinction coefficient (ϵ_{405}) for the heme−HO complexes was determined as previously described (*19*).

Circular Dichroism Spectrophotometry of the Wild-Type and nm-HO Mutant Complexes. Circular dichroism spectra were measured on a JASCO J-810 spectropolarimeter in the far-UV region (190−250 nm, 0.2 nm resolution, 1.0 nm bandwidth) at 25 °C in 10 mM potassium phosphate buffers at pH 6.0, 8.0, or 10.0 with a protein concentration of 5 μM. The molar ellipticities (degrees square centimeter per decimole) in the far-UV region were calculated directly using the JASCO standard software analysis following subtraction of the baseline spectra.

Reaction of the Heme−nm-HO Complexes with NADPH Cytochrome P450 Reductase. The reaction of the heme−HO complexes in the presence of NADPH reductase were carried out as previously described (*2*, *20*). Purified human cytochrome P450 reductase was added to the heme−HO complex (10 mM) at a reductase:HO molar ratio equal to 3:1 in a final volume of 1 mL of 20 mM Tris-HCl (pH 7.5). The reaction was initiated by the addition of NADPH in 10 mM increments to a final concentration of 100 mM. The spectral changes between 300 and 750 nm were monitored over a 30 min time period at 1 min intervals. Following completion of the reaction, the product was extracted for HPLC analysis as described previously (*21*).

Resonance Raman and FTIR Spectroscopy. Resonance Raman (RR) spectra were obtained on a McPherson 2061/207 spectrograph (0.67 m with variable gratings) equipped with a Princeton Instruments liquid N_2-cooled CCD detector (LN-1100PB). Kaiser Optical supernotch filters were used to attenuate Raleigh scattering. A Krypton laser (Innova 302) and a He/Cd laser (Liconix 4240NB) were used for the 413 and 442 nm excitations, respectively. Spectra were collected in a 90°-scattering geometry on samples at room temperature. Frequencies were calibrated relative to indene and CCl_4 and are accurate at ± 1 cm^{-1}. FTIR spectra were collected on a Perkin-Elmer System 2000 equipped with a liquid N_2-cooled MCT detector. The protein CO/complex solutions were sandwiched between two CaF_2 windows with a 0.05 mm spacer and mounted to a copper cell thermostated at 15 °C.

Preparation of HOs Reconstituted with ^{13}C-Labeled Heme. ^{13}C-labeled δ-aminolevulinic acids (ALAs) were used as biosynthetic precursors in the preparation of ^{13}C-labeled heme (Figure 2). [1,2-^{13}C]-δ-Aminolevulinic acid ([1,2-^{13}C]ALA) and [5-^{13}C]ALA were synthesized utilizing methods described previously (*22*). Heme labeled with ^{13}C was obtained by utilizing a previously reported methodology (*23*), developed to take advantage of the fact that the first committed precursor in heme biosynthesis is δ-aminolevulinic acid (ALA) (*24*, *25*). Thus, ^{13}C-labeled heme, which is biosynthesized in *E. coli* upon addition of suitably labeled ALA, is trapped by simultaneously expressing rat liver outer mitochondrial membrane cytochrome b_5 (OM cyt b_5) (*23*). The details of the biosynthetic protocol, which entails the expression and purification of OM cyt b_5 harboring ^{13}C-labeled heme, have been described previously (*26*). Reconstitution of HO with ^{13}C-labeled heme entails the removal of the isotopically labeled macrocycle from OM cyt b_5, followed by the reconstitution of HO with the purified [^{13}C]-heme to give the [^{13}C]heme−HO complex. A typical protocol used to extract ^{13}C-labeled heme from OM cyt b_5 follows: Pyridine (15 mL) is added to 2.5 mL of 1 mM OM cyt b_5 in phosphate buffer (μ = 0.10, pH 7.0). Slow addition of chloroform, typically 10−12 mL, results in the precipitation of the polypeptide, while maintaining the pyridine hemochrome in the supernatant. The latter is subsequently separated from the denatured polypeptide by centrifugation and then dried over anhydrous $MgSO_4$. The desiccant is removed by filtration and the filtered pyridine/chloroform

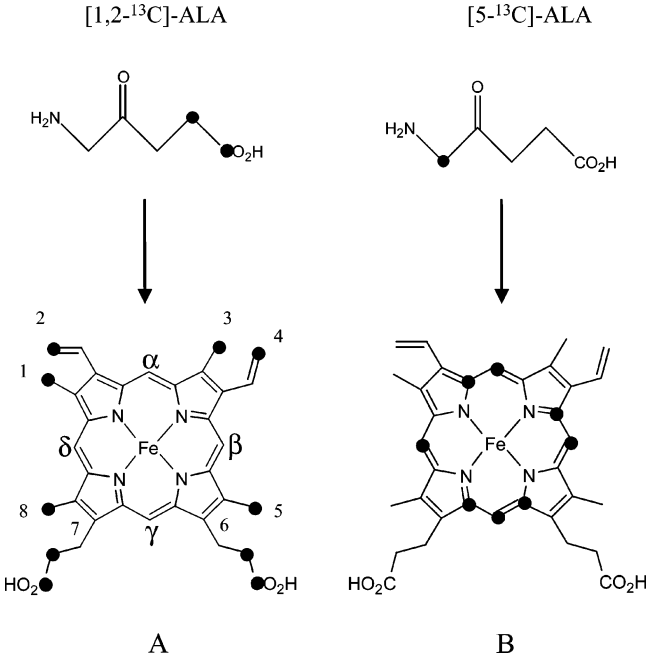

FIGURE 2: (A) ^{13}C labeling pattern obtained when protoporphyrin IX is biosynthesized from [1,2-^{13}C]ALA. (B) ^{13}C labeling pattern obtained when protoporphyrin IX is biosynthesized from [5-^{13}C]-ALA. The ● symbols represent positions labeled with ^{13}C.

solution transferred to a round-bottomed flask, where it is concentrated to dryness on a rotary evaporator. The solid is redissolved in 1.5 mL of dimethyl sulfoxide, and HO is reconstituted with a freshly prepared solution of ^{13}C-labeled heme by titrating it into a 25 mL solution of phosphate buffer (μ = 0.10, pH 7.0) containing ~2 μmol of HO until the A_{280}/A_{Soret} ratio no longer changes. The resultant solution is incubated at 4 °C overnight, then purified by size exclusion chromatography with the aid of a Sephadex G-50 column (90 cm × 2.6 cm, i.d.), equilibrated, and eluted with phosphate buffer (μ = 0.10, pH 7.0). Those fractions containing pure protein were concentrated in Amicon centrifugal concentrators to approximately 1 mL and then transferred to smaller Centricon concentrators to exchange the protein into deuterated phosphate buffer (pH 7.0, not corrected for the deuterium isotope effect).

NMR Spectroscopy of HOs. ^1H and ^{13}C spectra were acquired on a Varian Unity Inova spectrometer operating at frequencies of 599.740 (^1H) and 150.817 (^{13}C) MHz, respectively. ^1H spectra were referenced to the residual water peak at 4.8 ppm, and ^{13}C spectra were referenced to an external solution of dioxane [60% (v/v) in D_2O] at 66.66 ppm. Proton spectra were acquired with presaturation of the residual water peak over 10K data points, with a spectral width of 30 kHz, a 150 ms acquisition time, a 200 ms relaxation delay, and 1024 scans. ^{13}C spectra were collected over 12K data points, with a spectral width of 60 kHz, a 100 ms acquisition time, a 25 ms relaxation delay, and 400 000 scans. HMQC spectra (*27*) were typically acquired with spectral widths of 30 kHz for ^1H and 50 kHz for ^{13}C and a 200 ms relaxation delay. HMQC spectra obtained from samples containing HOs reconstituted with heme labeled using [1,2-^{13}C]ALA as a heme precursor (Figure 2A) were acquired with refocusing delays based on a $^1J_{CH}$ of 140 Hz, while data obtained from HOs reconstituted with heme labeled using [5-^{13}C]ALA as the heme precursor (Figure 2B) were acquired with a $^1J_{CH}$ of 180 Hz. Data were collected as an array of 2K × 128 points with 320 scans per t_1 increment and processed by zero filling in both t_1 and t_2 dimensions to obtain a 4K × 4K matrix. This was apodized with a 90°-shifted squared sine bell function and Fourier transformed. WEFT−NOESY (*28*, *29*) spectra were acquired with 30 kHz in both dimensions, 2K data points in t_2, 256 increments in t_1, 352 scans per t_1 increment, and (typically) a 40 ms mixing time. The data were processed by zero filling in both dimensions to obtain a 4K × 4K matrix, apodized with a 90°-shifted squared sine bell function, and Fourier transformed. EXSY (*30*) spectra were acquired in a similar manner except that the mixing time was set to 10 ms.

RESULTS AND DISCUSSION

Expression, Purification, and Spectral Characterization of the nm-HOch and nm-HO Mutants. The wild-type enzyme and the *nm*-HO mutant proteins were expressed and purified as described previously (*1*, *2*). All of the proteins were judged to be >95% pure by SDS−PAGE (data not shown). The Soret maxima of the resting state (Fe^{III}) wild-type heme−*nm*-HO and heme−*nm*-HO mutant proteins are very similar, ranging from 404 to 406 nm (Table 1). The Soret maxima for the Fe^{II}−CO complex of the wild-type, *nm*-HO K16A, and chimeric proteins ranged from 421 to 422 nm, and those for the the $Fe^{II}-O_2$ complexes were at 410 nm (Table 1 and Figure 3A). The CD spectra of wild-type *nm*-HO, *pa*-HO, and *nm*-HOch are shown in Figure 3B. All three spectra show significant α-helical content, consistent with the crystal structure of *nm*-HO. In addition, the *nm*-HOch protein, as judged by the increased 220 nm intensity, shows an increase in α-helical content, which approximates that of wild-type *pa*-HO.

Resonance Raman (RR) spectra obtained from the reduced heme−protein complexes of wild-type *nm*-HO and *nm*-HOch confirm that the interactions between the heme iron and the proximal histidine are unperturbed (Figure 4). Both complexes exhibit high-frequency RR spectra characteristic of a pentacoordinate ferrous high-spin heme with an intense signal at 220 ± 1 cm^{-1} distinctive of an iron−histidine stretching frequency (*31*). The ν(Fe−His) is known to be sensitive to hydrogen bond interactions involving the proximal histidine and the orientation of the imidazole ring with respect to the tetrapyrrole axis; the similarity in frequencies clearly indicates that the environment of the proximal histidine is nearly unchanged in the *nm*-HOch heme complex.

To further examine the heme distal pocket environment, the ferrous−CO complexes were investigated using FTIR spectroscopy. In porphyrin model compounds and hemoproteins, the [Fe−C≡O] band is known to be a sensitive probe of the proximal and distal environment of the heme group (*32*) and has been used extensively in studying myoglobin distal pocket variants (*33*, *34*). The chimeric protein, *nm*-HOch, has a heme−CO complex with a ν(C≡O) at 1951 cm^{-1} (Figure 5). This frequency is within 3 cm^{-1} of that observed in *pa*-HO, but 13 cm^{-1} lower than in the *nm*-HO wild-type protein complex (Figure 5). Since all three heme−CO complexes share the same proximal ligand, namely, a neutral histidine, the downshift of the ν(C≡O) in *nm*-HOch can be assigned to an increase in the extent of hydrogen bond interactions by the carbonyl moiety

Table 1: Comparison of the Electronic Absorption Features of the Wild-Type *nm*-HO and *nm*-HOch Complexes

enzyme	Soret maxima (nm)			visible bands (nm)			Soret extinction coefficient (mM^{-1} cm^{-1})
	Fe^{III}	$Fe^{II}-O_2$	$Fe^{II}-CO$	Fe^{III}	$Fe^{II}-O_2$	$Fe^{II}-CO$	
wild-type	405	410	421	630	568/538	570/539	170
nm-HOch	406	410	422	630	574/539	570/540	149
nm-HOch K16A	406	410	422	630	575/540	575/539	139
nm-HOch K16A/M31K	405	410	422	630	576/539	570/540	146

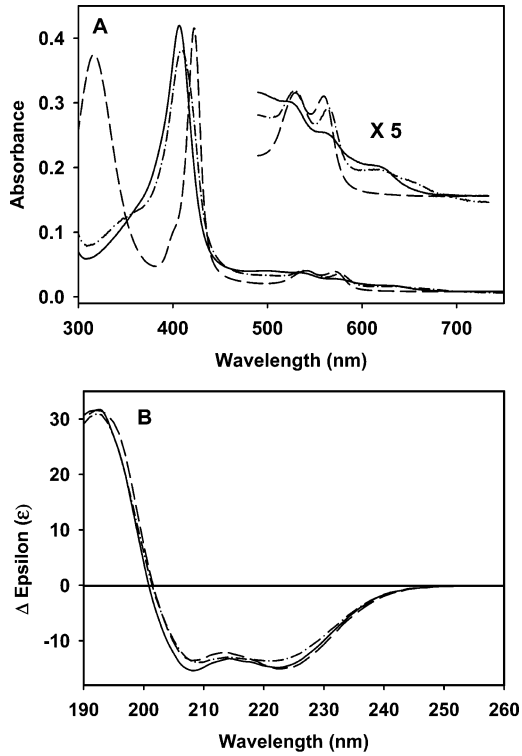

FIGURE 3: (A) Electronic absorption spectra of *nm*-HOch: $Fe^{III}-$heme complex (—), $Fe^{II}-$CO heme complex (– – –), and $Fe^{II}-O_2$ complex (—•—). Spectra were recorded in 20 mM Tris (pH 7.5). (B) Circular dichroism spectra of *nm*-HOch (—), *nm*-HO (—•—), and *pa*-HO (– – –). Spectra were recorded in 10 mM potassium phosphate buffer (pH 7.5).

and/or an increase in the electrostatic potential of the distal pocket. Changes in the distal pocket of the chimeric protein are also implicated in the plots relating the percentage of dissociation of the high-spin $Fe^{III}-H_2O$ complex to the low-spin $Fe^{III}-OH$ complex for wild-type *nm*-HO, *pa*-HO, and *nm*-HOch (Figure 6B). Wild-type *nm*-HO exhibits a pK_a of 9.2, whereas that measured for *nm*-HOch, at 8.3, is closer to the pK_a of 8.0 measured for *pa*-HO. The shift in the pK_a of *nm*-HOch toward that of *pa*-HO, together with the electronic absorption, FTIR, and Raman spectral characteristics, indicates that the distal pocket environment in *nm*-HOch is similar in nature to that of *pa*-HO, rather than that of *nm*-HO.

Catalytic Turnover of the nm-HO Mutant Proteins. As previously reported, the NADPH cytochrome P450 reductase-supported catalytic oxidation of heme by *nm*-HO yields α-biliverdin as the sole product (Table 2). The *nm*-HO chimera (*nm*-HOch), in which the distal helix residues of *nm*-HO were replaced with those of *pa*-HO, gave α-biliverdin as the primary product of the reaction with a detectable and reproducible fraction of δ-biliverdin (Table 2). As will be described below, the altered regioselectivity in *nm*-HOch is a result of a dynamic in-plane rotation of the heme.

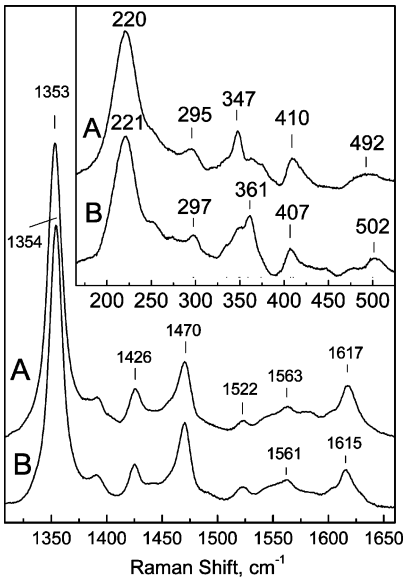

FIGURE 4: High-frequency region of the RR spectra of ferrous heme−protein complexes in *nm*-HO (A) and *nm*-HOch (B). The inset shows the low-frequency region obtained with a 442 nm excitation.

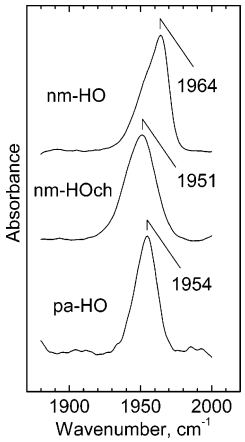

FIGURE 5: FTIR spectra in the 1900−2000 cm^{-1} region of the heme−CO complex formed in *nm*-HO, *nm*-HOch, and *pa*-HO.

Furthermore, the discrepancy between the percentage of δ-biliverdin produced in the chimeric protein and that predicted from the NMR studies, as will be described below, is most likely due to the slight difference in heme orientation (approximately 10°) between *nm*-HOch and wild-type *pa*-HO. The result of this slight difference in heme orientation is that it introduces increased steric hindrance in the chimeric protein such that the δ-meso carbon is less reactive. Therefore, the resulting channeling of the reactivity through the more competent α-selective heme seating is responsible for the amount of δ-biliverdin being smaller than that expected from the NMR data. To investigate this phenomenon in more detail, we incorporated two additional muta-

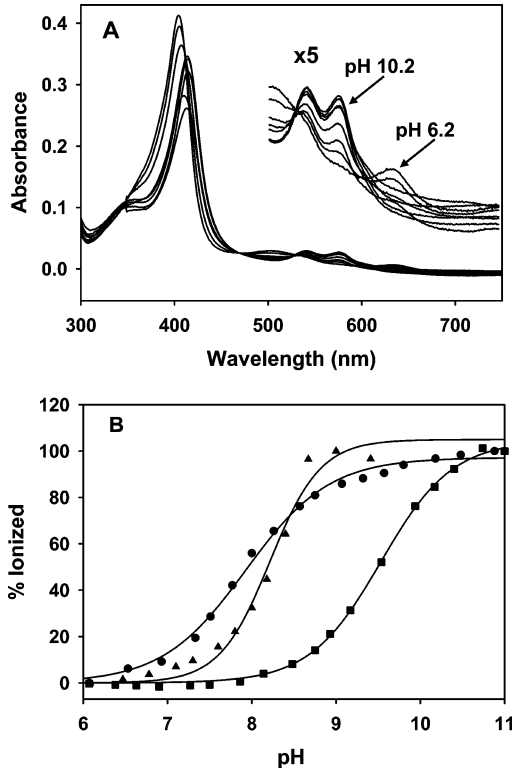

FIGURE 6: (A) Electronic absorption spectra of the *nm*-HO−heme complex as a function of pH. pH-dependent changes in absorption were brought about by incremental addition of NaOH to a solution of $Fe^{III}-H_2O$ heme *nm*-HO in 20 mM Tris. (B) The pK_a for the transition from the high-spin $Fe^{III}-H_2O$ complex to the low-spin $Fe^{III}-OH$ complex was measured by following the absorption at 404 nm and by fitting the data to the Henderson−Hasselbach equation: wild-type *pa*-HO (●), *nm*-HO (■), and *nm*-HOch (▲).

Table 2: Regioselectivity of Heme Oxygenation in *nm*-HO and *nm*-HOch[a]

	biliverdin isomer ratio (%)			
nm-HO protein	α	*β*	*δ*	*γ*
wild-type	100	0	0	0
nm-HOch	95	0	5	0
nm-HOch K16A	65	0	35	0
nm-HOch K16A/M31K	5	0	95	0

[a] The percentage of each isomer was obtained by integration of the peaks within each chromatogram. The reported values are an average obtained from five separate experiments. The standard deviation is ±5%.

tions, *nm*-HOch K16A and *nm*-HOch K16A/M31K, in an attempt to engineer heme propionate−polypeptide interactions aimed at stabilizing the in-plane heme conformation conducive to *δ*-meso carbon hydroxylation (see Table 2). The results obtained from these studies (discussed in the following section) demonstrate that the introduction of key polypeptide−heme propionate contacts permits the construction of a chimeric enzyme that oxidizes heme to mostly (95%) *δ*-biliverdin.

NMR Spectroscopic Studies. The wild-type and chimera proteins were converted to the corresponding low-spin cyanide-inhibited forms to facilitate their investigation by NMR spectroscopy. Unambiguous assignment of ^1H and ^{13}C resonances originating from the heme active site of *nm*-HO and *nm*-HOch was facilitated by well-documented strategies (*12*, *13*, *36*) that utilize judicious labeling of the heme

Table 3: ^1H and ^{13}C NMR Chemical Shifts for the Wild-Type *nm*-HO−CN Complex (30 °C and pH 7.0)

position	^1H (ppm)	^{13}C (ppm)
1-Me	8.19	−17.41
3-Me	21.12	−47.68
5-Me	9.80	−22.36
8-Me	10.27	−24.26
2-Vα	14.64	−
2-V*β*	−5.18, −6.18	194.08
4-Vα	8.26	−
4-V*β*	−2.51, −3.11	151.60
meso-α	−1.70	44.97
meso-*β*	8.40	4.55
meso-*γ*	−1.32	27.30
meso-*δ*	7.19	22.22
6-P-α	1.61, 16.83	−
6-P-*β*	−0.72, −2.93	116.41
7-P-α	5.79, 12.92	−
7-P-*β*	−0.97, −2.05	104.48

macrocycle. The latter was accomplished by carefully positioning the ^{13}C label in the heme precursor *δ*-aminolevulinic acid. Hence, heme labeled at four methyl, two vinyl-*β*, two propionate-*β*, and two carbonyl carbon (Figure 2A) was obtained from [1,2-^{13}C]-*δ*-aminolevulinic acid ([1,2-^{13}C]-ALA), and heme labeled at the meso carbons was prepared from [5-^{13}C]ALA (Figure 2B). Chemical shifts corresponding to ^1H and ^{13}C nuclei in the heme macrocycle were identified with a combination of one-dimensional nondecoupled ^{13}C and two-dimensional HMQC spectra. The ^1H resonance assignments were subsequently obtained from a NOESY map (Figure S1 of the Supporting Information). The resonance assignments obtained in this manner (30 °C) for the wild-type *nm*-HO−CN complex (Table 3) are in good agreement with those previously reported at 25 °C (*35*).

The high-frequency portion of the ^1H NMR spectrum corresponding to the *nm*-HOch−CN complex (Figure 7C) shows several new peaks between 9 and 26 ppm when compared to the ^1H NMR spectrum of the wild-type *nm*-HO−CN (Figure 7A) or *pa*-HO−CN (Figure 7B) complex. The presence of these new peaks in the ^1H NMR spectrum is suggestive of in-plane heme disorder (*12*, *13*). Assignment of these resonances, summarized in Table 4, was accomplished using the strategy outlined above and the dipolar connectivities in the WEFT−NOESY spectrum shown in Figure 8. In this manner, the methyl ^1H resonances at 20.35, 12.95, 10.36, and 6.40 ppm were identified to correspond to the 3-Me, 8-Me, 5-Me, and 1-Me groups, respectively (see Figure 7C), in heme conformer I.

As has been pointed out above, our previous work with HO has shown that heme in these enzymes can readily rotate in plane by as much as 100° (*12*, *13*). It was therefore conceivable that the less intense set of not yet assigned heme methyl ^1H resonances could be correlated to the heme methyl resonances of conformer I by exchange spectroscopy (EXSY). Indeed, the EXSY spectrum of the *nm*-HOch−CN complex (Figure 9) demonstrates that each of the four methyl resonances from heme conformer I exhibits a strong exchange cross-peak with resonances identified to originate from heme methyl protons in an HMQC spectrum. These exchange connectivities (summarized below) permit the assignment of heme methyl resonances in heme conformer II (see Figure 7C). Taken together, these observations suggest a dynamic exchange between two in-plane heme conformers

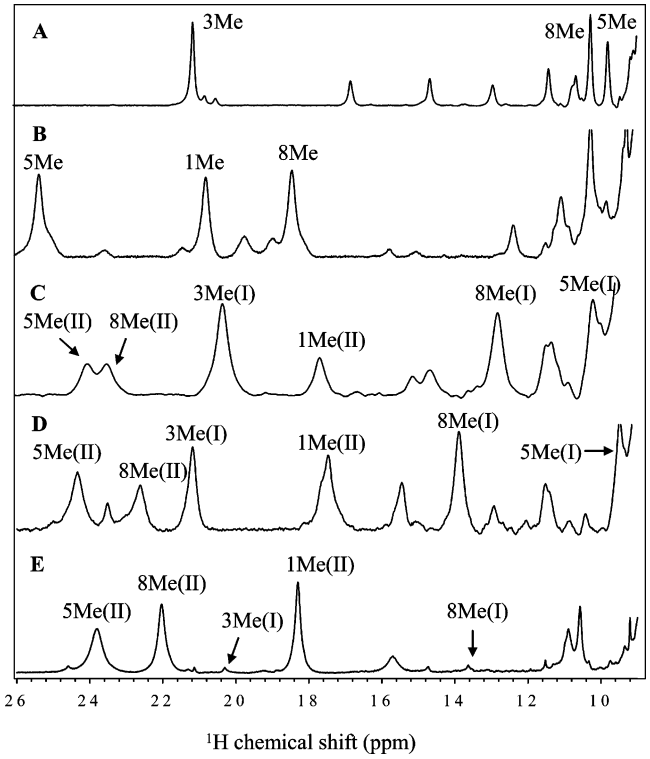

FIGURE 7: Downfield portion of the ^{1}H NMR spectra of cyanide-inhibited (A) *nm*-HO, (B) *pa*-HO, (C) *nm*-HOch, (D) *nm*-HOch K16A at 30 °C and (E) *nm*-HOch K16A/M31K at 35 °C.

that is similar to exchange we observed with mutants of the bacterial *pa*-HO and *cd*-HO (*12*, *15*).

conformer I		conformer II
3-Me(I) 20.35 ppm	⇄	3-Me(II) 8.37 ppm
8-Me(I) 12.95 ppm	⇄	8-Me(II) 23.43 ppm
5-Me(I) 10.36 ppm	⇄	5-Me(II) 24.14 ppm
1-Me(I) 6.40 ppm	⇄	1-Me(II) 17.70 ppm

The plot in Figure 10 shows the pattern of isotropic shifts predicted for heme methyl groups as a function of the angle (Φ) between the axial ligand plane and the molecular *x* axis (*37*). The order of methyl ^{1}H chemical shifts exhibited by the wild-type *nm*-HO−CN complex at 30 °C is as follows: 3-Me > 8-Me > 5-Me > 1-Me (21.12, 10.27, 9.80, and 8.19 ppm, respectively; Table 4). In the context of the plot of Figure 10, this pattern suggests a Φ angle of approximately 135°. This angle is in good agreement with that observed in the crystal structure of *nm*-HO (*10*). The relative intensity of the methyl peaks originating from conformer I in the *nm*-HOch−CN protein (see Figure 7C) clearly indicates that this is the predominant conformer in solution (~70% abundance). Further, the methyl ^{1}H chemical shifts originating from this species are similar to those observed in the spectrum of wild-

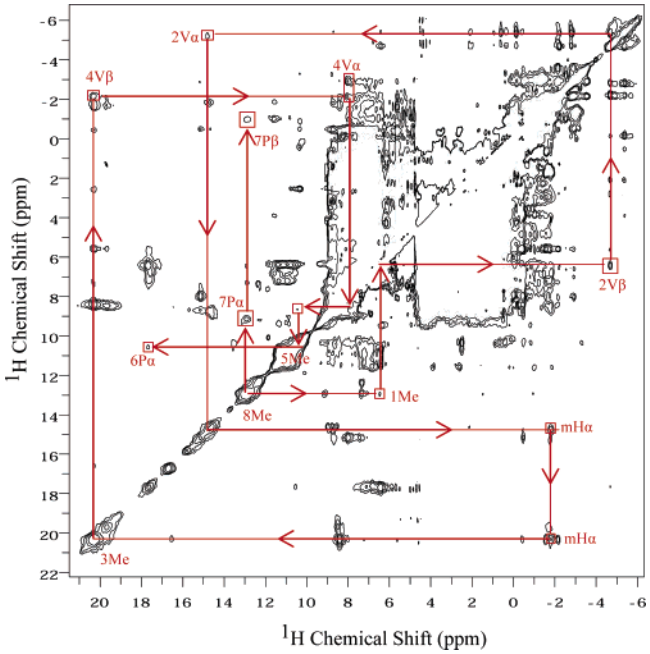

FIGURE 8: WEFT−NOESY spectrum of cyanide-inhibited *nm*-HOch at 30 °C. The dipolar connectivities between the heme resonances from conformer I are similar to that observed in the NOESY spectrum of the *nm*-HO−CN complex (Figure S1) and can be traced as follows: 8-Me → 1-Me → 2-V_β → 2-V_α → meso-H_α → 3-Me → 4-V_β → 4-V_α → 5-Me → 6-P_α. 7-P_α and 7-P_β can be recognized by their cross-peaks with 8-Me.

type *nm*-HO (Table 4), which suggests that the in-plane conformation of I is similar to that seen in the wild-type enzyme, where the Φ angle is 135°. This in-plane conformation of the heme in *nm*-HOch is expected to place the α-meso carbon in a position where it is susceptible to hydroxylation, which is consistent with the catalytic formation of mostly α-biliverdin (Table 2). In comparison, the order of heme methyl ^{1}H chemical shifts obtained for conformer II in *nm*-HOch (5-Me > 8-Me > 1-Me > 3-Me) suggests an angle of ~45°. This finding indicates that conformers I and II are related to one another by a ~95° in-plane rotation of the heme, as has been schematically illustrated in Scheme 1. This dynamic equilibrium between the two in-plane heme conformers is clearly manifested in the exchange cross-peaks of the EXSY spectrum in Figure 9. A consequence of in-plane heme rotation is that the macrocycle adopts an orientation similar to that observed in wild-type *pa*-HO, where the two propionate groups are exposed to the aqueous environment (Scheme 1 and Figure 1A). Previous NMR spectroscopic (*12*) and X-ray crystallographic (*13*) studies demonstrated that the Φ angle in wild-type *pa*-HO is 33°. This in-plane conformation places the *δ*-meso carbon where it is susceptible to hydroxylation, thus explaining the unusual

Table 4: Heme Methyl ^{1}H Chemical Shifts (parts per million) at 30 °C and pH 7.0

			nm-HOch−CN		*nm*-HOch K16A−CN		*nm*-HOch K16A/M31K−CN	
position	*nm*-HO−CN	*pa*-HO−CN	I	II	I	II	I	II
1-Me	8.19	20.80	6.40	17.70	5.78	17.56	8.33	18.32
3-Me	21.12	4.41	20.35	8.37	21.24	8.62	22.32	8.09
5-Me	9.80	25.34	10.36	24.14	9.64	24.34	9.82	23.84
8-Me	10.27	18.46	12.95	23.43	13.99	22.67	13.64	22.04
order	3 > 8 ≈ 5 > 1	5 > 1 ≈ 8 > 3	3 > 8 > 5 > 1	5 > 8 > 1 > 3	3 > 8 > 5 > 1	5 > 8 > 1 > 3	3 > 8 > 5 > 1	5 > 8 > 1 > 3
Φ (deg)	~135	~35	~130	~45	~130	~45	~130	~40

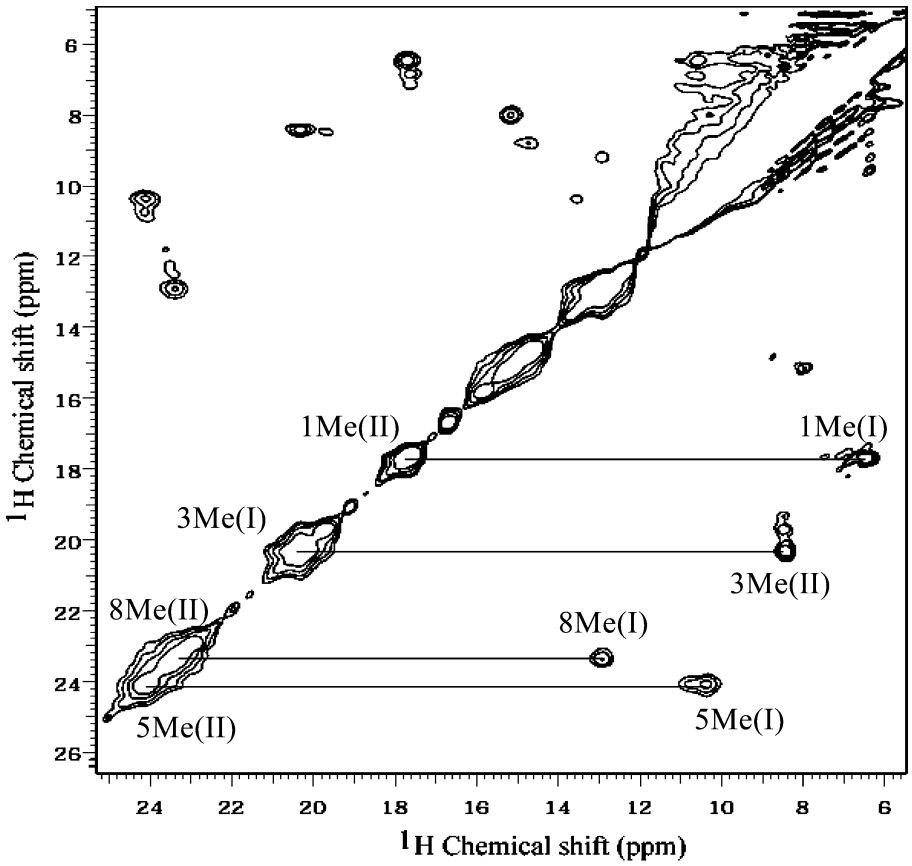

FIGURE 9: EXSY spectrum of *nm*-HOch−CN complex at 30 °C showing the dynamic exchange between conformer I and conformer II.

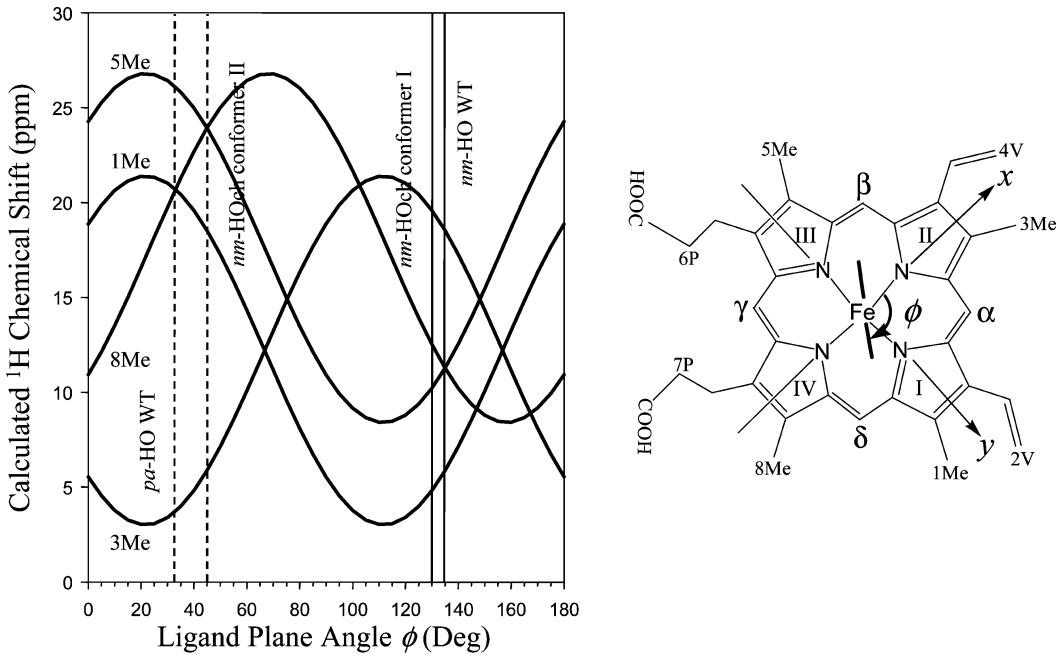

FIGURE 10: Plot illustrating the dependence of the heme methyl chemical shifts on the Φ angle made by the projection of the proximal histidine−imidazole plane and the molecular *x*-axis. Conformer I in *nm*-HOch exhibits a Φ angle similar to that characteristic of *nm*-HO, whereas conformer II exhibits a Φ angle of 45°, which is 10° larger than that characteristic of *pa*-HO.

production of δ-biliverdin by this enzyme. It is therefore possible that the 10° difference in the in-plane heme orientation observed between *nm*-HOch (Φ = 45°) and wild-type *pa*-HO (Φ = 35°) places the δ-meso carbon of conformer II in *nm*-HOch in a position where it is sterically protected from attack by the terminal OH in the Fe^{III}−OOH oxidizing species. Consequently, δ-hydroxylation is less efficient, which would account for the formation of only 5% δ-biliverdin, despite the presence of a >5% equilibrium population of conformer II (see Figure 7C). The dynamic equilibrium between I and II, on the other hand, replenishes I and channels the reaction toward the oxidation of conformer I, which results in the formation of mainly α-biliverdin. In this context, it is important to point out that X-ray

Scheme 1

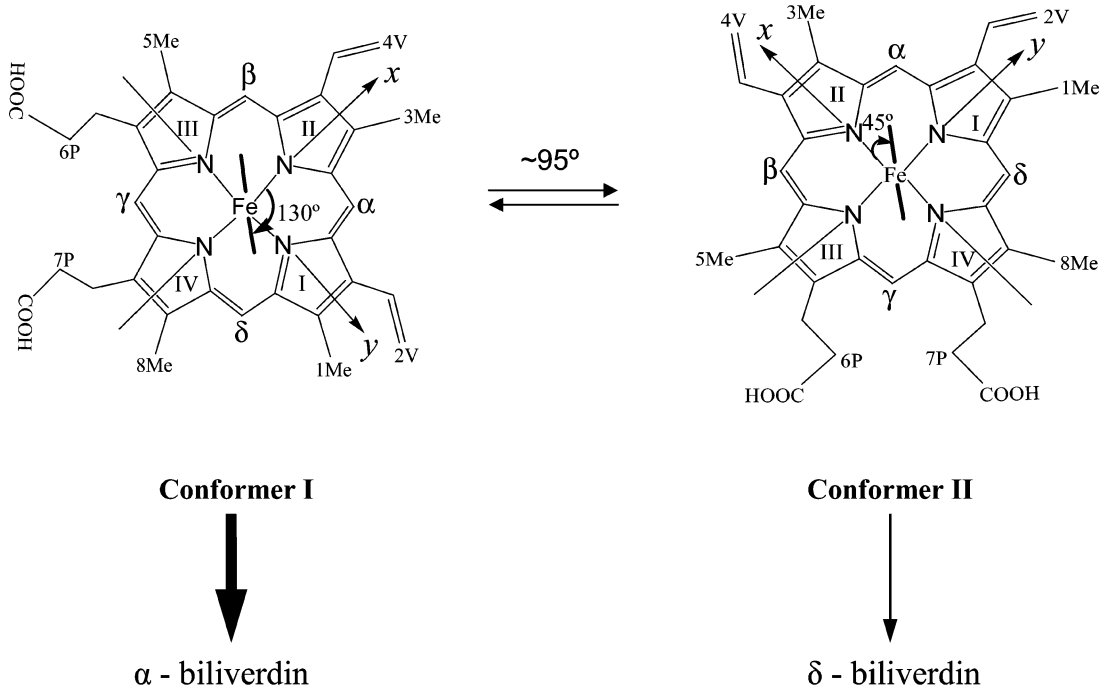

crystal structures (*7*, *11*) suggest steric interactions in the distal pocket of HO that steer the HOO^- ligand to lie almost on top of the meso carbon susceptible to hydroxylation: α-meso in α-biliverdin-producing enzymes and *δ*-meso in the *δ*-biliverdin-producing *pa*-HO (*12*, *13*). Hence, it is reasonable that if the in-plane heme rotation observed in the *nm*-HOch protein does not position the *δ*-meso carbon where it can be readily attacked by the $Fe^{III}-OOH$ moiety, oxidation of the *δ*-meso carbon would be inefficient. We have previously observed the same phenomenon in the *cd*-HO R177E mutant, where the reaction is channeled toward formation of 55% *δ*-biliverdin while the percentage of the heme rotational conformer predicted from the NMR data suggests only 5% *δ*-biliverdin would be produced (*15*).

Organizing the Active Site by Building Stabilizing Heme Propionate−Polypeptide Contacts. Previous work with *pa*-HO mutants showed that replacing Phe-117 with Tyr and Asn-119 with Lys leads to heme in-plane disorder as a consequence of promoting stabilizing contacts between these side chains and the heme propionates (*12*), in addition to those built in the wild-type protein for stabilization of the wild-type heme seating. Subsequently, the crystal structure of *pa*-HO showed that the wild-type seating is stabilized by electrostatic interactions between the heme propionates and Lys-34 and Lys-132 (*13*) (see Figure 1). Construction of *nm*-HOch replaced Tyr-112 with Phe, the equivalent of Phe-117 in *pa*-HO. However, the chimeric protein still harbors Lys at position 16, which may account for stabilizing the heme in an in-plane conformation that is conducive to α-meso hydroxylation. In addition, although *nm*-HOch contains the equivalent of Lys-132, the residue equivalent to Lys-34 is Met. It is therefore possible that in-plane heme disorder in *nm*-HOch is a consequence of interactions that lead to the stabilization of both the α-hydroxylating (Lys-16) and *δ*-hydroxylating (Lys-127) seatings. This hypothesis was tested by preparing two mutants of the chimeric protein, *nm*-HOch K16A and *nm*-HOch K16A/M31K.

The number of peaks in the downfield portion of the NMR spectrum corresponding to the *nm*-HOch K16A mutant (Figure 7D) suggests that the heme in this protein samples at least two in-plane conformations. ^{13}C labeling of the heme methyl groups facilitated identification of these resonances; a WEFT−NOESY spectra allowed assignment of the heme methyl ^1H resonances in conformer I, and an EXSY (Figure S2 of the Supporting Information) spectrum facilitated assignment of the heme methyl ^1H resonances in conformer II (Table 4). The relative populations of conformers I and II inferred from the ^1H NMR spectrum would suggest the formation of approximately 50% *δ*- and α-biliverdin, a prediction that approximates the 35% *δ*-biliverdin formed by *nm*-HOch K16A (Table 2). Hence, the data are consistent with the notion that replacing Lys-16 with Ala eliminates a stabilizing interaction that promotes the heme seating conducive to α-meso hydroxylation. However, the ^1H NMR (Figure 7D) and EXSY (Figure S2 of the Supporting Information) spectra of *nm*-HOch K16A clearly demonstrate that substantial in-plane heme disorder still exists. Moreover, the formation of less *δ*-biliverdin than the amount predicted from the relative abundance of the two heme seatings, as predicted from the NMR spectrum, suggests that oxidation of the *δ*-meso carbon remains relatively inefficient. In this context, it is interesting that the *nm*-HOch K16A/M31K forms 95% *δ*-biliverdin (Table 2) and displays a ^1H NMR spectrum (Figure 7E) that exhibits three heme methyl peaks resolved from the diamagnetic envelope of resonances. The magnitude and order of these resonances suggest a Φ angle of ∼40°, which is similar to that of wild-type *pa*-HO. Closer inspection of the ^1H NMR spectrum of Figure 7E reveals the presence of small peaks, likely originating from the alternative in-plane heme conformation (conformer I) which would account for the small fraction of α-biliverdin produced (Table 2). Labeling the heme methyl groups with ^{13}C demonstrates that these peaks split into doublets. In addition, the EXSY spectrum of Figure S3 of the Supporting Information demon-

strates that the in-plane heme conformation (conformer I) that gives rise to these low-intensity heme methyl resonances is in dynamic exchange with the more abundant conformer II. These findings allow us to conclude that the introduction of Lys-31 into the *nm*-HOch K16A mutant greatly stabilizes the in-plane conformation conducive to *δ*-meso hydroxylation, which is manifested in the dynamic exchange between heme conformers I and II and in the formation of 95% *δ*- and 5% α-biliverdin. It is also possible that the Φ angle (∼40°) in *nm*-HOch K16A/M31K approaches more closely that of wild-type *pa*-HO (Φ ∼ 35°) than those of the *nm*-HOch and *nm*-HO K16A mutants (Φ ∼ 45°), which relieves some of the steric hindrance and increases the efficiency of *δ*-regioselective oxidation.

Concluding Remarks. The findings reported herein demonstrate that replacement of the distal helix in *nm*-HO with that corresponding to *pa*-HO results in a fully active chimeric protein. This observation indicates that HO enzymes exhibit remarkable flexibility in their ability to tune structural elements in channeling the reactivity of the Fe^{III}−OOH intermediate toward heme hydroxylation. The NMR data on the chimera protein also underscore the dynamic flexibility of the heme binding site which allows large amplitude (∼95°) in-plane rotation of the heme on a time scale of less than 10 ms (the mixing time used in EXSY spectra). In-plane heme rotations such as those observed for the chimeric proteins are expected to be met with steric friction between heme substituents and polypeptide side chain and backbone. Thus, the ease with which large amplitude in-plane heme disorder can be brought about, typically by suboptimal interactions with the heme propionates, suggests a large degree of plasticity in the heme binding site of HO enzymes. The results presented herein also provide further evidence that the regioselectivity and reactivity of heme oxygenase is a dynamic interplay between steric restrictions driven by interactions of the heme propionates with the protein scaffold and modulation of the bound ligand by the hydrogen bond network, which allows the porphyrin deformation required to electronically configure the heme for hydroxylation.

SUPPORTING INFORMATION AVAILABLE

WEFT−NOESY spectrum of cyanide-inhibited *nm*-HO at 30 °C (Figure S1), EXSY spectrum of the *nm*-HOch K16A−CN complex at 30 °C (Figure S2), and EXSY spectrum of the *nm*-HOch K16A/M31K−CN complex at 35 °C (Figure S3). This material is available free of charge via the Internet at http://pubs.acs.org.

REFERENCES

1. Ratliff, M., Zhu, W., Deshmukh, R., Wilks, A., and Stojiljkovic, I. (2001) Homologues of Neisserial Heme Oxygenase in Gram-Negative Bacteria: Degradation of Heme by the Product of the pigA Gene of *Pseudomonas aeruginosa*, *J. Bacteriol. 183*, 6394−6403.
2. Zhu, W., Wilks, A., and Stojiljkovic, I. (2000) Degradation of Heme in Gram-Negative Bacteria: The Product of the hemO Gene of *Neisseriae meningitidis* Is a Heme Oxygenase, *J. Bacteriol. 182*, 6783−6790.
3. Wilks, A., and Moenne-Loccoz, P. (2000) Identification of the Proximal Ligand His-20 in Heme Oxygenase (Hmu O) from *Corynebacterium diphtheriae*. Oxidative cleavage of the heme macrocycle does not require the proximal histidine, *J. Biol. Chem. 275*, 11686−11692.
4. Schuller, D. J., Wilks, A., Ortiz de Montellano, P. R., and Poulos, T. L. (1999) Crystal structure of human heme oxygenase-1, *Nat. Struct. Biol. 6*, 860−867.
5. Lad, L., Wang, J., Li, H., Friedman, J., Bhaskar, B., Ortiz de Montellano, P. R., and Poulos, T. L. (2003) Crystal structures of the ferric, ferrous, and ferrous-NO forms of the Asp140Ala mutant of human heme oxygenase-1: Catalytic implications, *J. Mol. Biol. 330*, 527−538.
6. Sugishima, M., Omata, Y., Kakuta, Y., Sakamoto, H., Noguchi, M., and Fukuyama, K. (2000) Crystal structure of rat heme oxygenase-1 in complex with heme, *FEBS Lett. 471*, 61−66.
7. Sugishima, M., Sakamoto, H., Higashimoto, Y., Omata, Y., Hayashi, S., Noguchi, M., and Fukuyama, K. (2002) Crystal structure of rat heme oxygenase-1 in complex with heme bound to azide. Implication for regiospecific hydroxylation of heme at the α-meso carbon, *J. Biol. Chem. 277*, 45086−45090.
8. Sugishima, M., Sakamoto, H., Noguchi, M., and Fukuyama, K. (2003) Crystal structures of ferrous and CO-, CN^--, and NO-bound forms of rat heme oxygenase-1 (HO-1) in complex with heme: Structural implications for discrimination between CO and O_2 in HO-1, *Biochemistry 42*, 9898−9905.
9. Friedman, J., Lad, L., Deshmukh, R., Li, H., Wilks, A., and Poulos, T. L. (2003) Crystal structures of the NO- and CO-bound heme oxygenase from *Neisseriae meningitidis*. Implications for O_2 activation, *J. Biol. Chem. 278*, 34654−34659.
10. Schuller, D. J., Zhu, W., Stojiljkovic, I., Wilks, A., and Poulos, T. L. (2001) Crystal structure of heme oxygenase from the gram-negative pathogen *Neisseria meningitidis* and a comparison with mammalian heme oxygenase-1, *Biochemistry 40*, 11552−11558.
11. Unno, M., Matsui, T., Chu, G. C., Couture, M., Yoshida, T., Rousseau, D. L., Olson, J. S., and Ikeda-Saito, M. (2004) Crystal Structure of the Dioxygen-bound Heme Oxygenase from *Corynebacterium diphtheriae*: Implications for Heme Oxygenase Function, *J. Biol. Chem. 279*, 21055−21061.
12. Caignan, G. A., Deshmukh, R., Wilks, A., Zeng, Y., Huang, H. W., Moenne-Loccoz, P., Bunce, R. A., Eastman, M. A., and Rivera, M. (2002) Oxidation of heme to *β*- and *δ*-biliverdin by *Pseudomonas aeruginosa* heme oxygenase as a consequence of an unusual seating of the heme, *J. Am. Chem. Soc. 124*, 14879−14892.
13. Friedman, J., Lad, L., Li, H., Wilks, A., and Poulos, T. L. (2004) Structural basis for novel *δ*-regioselective heme oxygenation in the opportunistic pathogen *Pseudomonas aeruginosa*, *Biochemistry 43*, 5239−5245.
14. Fujii, H., Zhang, X., and Yoshida, T. (2004) Essential Amino Acid Residues Controlling the Unique Regioselectivity of Heme Oxygenase in *Pseudomonas aeruginosa*, *J. Am. Chem. Soc. 126*, 4466−4467.
15. Zeng, Y., Deshmukh, R., Caignan, G. A., Bunce, R. A., Rivera, M., and Wilks, A. (2004) Mixed regioselectivity in the Arg-177 mutants of *Corynebacterium diphtheriae* heme oxygenase as a consequence of in-plane heme disorder, *Biochemistry 43*, 5222−5238.
16. Sambrook, J., Fritsch, E. F., and Maniatis, T. (1989) *Molecular Cloning: A Laboratory Manual*, Cold Spring Harbor Laboratory Press, Plainview, NY.
17. Yoshida, T., and Kikuchi, G. (1979) Purification and properties of heme oxygenase from rat liver microsomes, *J. Biol. Chem. 254*, 4487−4491.
18. Wilks, A., and Ortiz de Montellano, P. R. (1993) Rat liver heme oxygenase. High level expression of a truncated soluble form and nature of the meso-hydroxylating species, *J. Biol. Chem. 268*, 22357−22362.
19. Fuhrop, J. H., and Smith, K. M. (1975) (Smith, K. M., Ed.) pp 804−807, Elsevier, Amsterdam.
20. Wilks, A., and Schmitt, M. P. (1998) Expression and characterization of a heme oxygenase (Hmu O) from *Corynebacterium diphtheriae*. Iron acquisition requires oxidative cleavage of the heme macrocycle, *J. Biol. Chem. 273*, 837−841.
21. Sakamoto, H., Omata, Y., Adachi, Y., Palmer, G., and Noguchi, M. (2000) Separation and identification of the regioisomers of verdoheme by reversed-phase ion-pair high-performance liquid chromatography, and characterization of their complexes with heme oxygenase, *J. Inorg. Biochem. 82*, 113−121.
22. Bunce, R. A., Shilling, C. L., III, and Rivera, M. (1997) Synthesis of [1,2-^{13}C]- and [2,3-^{13}C]-Labeled *δ*-Aminolevulinic Acid, *J. Labelled Compd. Radiopharm. 39*, 669−675.

23. Rivera, M., and Walker, F. A. (1995) Biosynthetic Preparation of Isotopically Labeled Heme, *Anal. Biochem. 230*, 295−302.
24. Warren, M. J., and Scott, A. I. (1990) Tetrapyrrole Assembly and Modification into the Ligands of Biologically Functional Cofactors, *Trends Biochem. Sci. 15*, 426−431.
25. Scott, A. I. (1993) How Nature Synthesizes Vitamin B_{12}: A Survey of the Last Four Billion Years, *Angew. Chem. 32*, 1223−1376.
26. Rivera, M., Qiu, F., Bunce, R. A., and Stark, R. E. (1999) Complete Isomer-Specific ^{1}H and ^{13}C NMR Assignments of the Heme Resonances of Rat Liver Outer Mitochondrial Membrane Cytochrome b_5, *J. Biol. Inorg. Chem. 4*, 87−98.
27. Summers, M. F., Marzilli, L. G., and Bax, A. (1986) Complete ^{1}H and ^{13}C Assignments of Coenzyme B_{12} through the Use of New Two-Dimensional NMR Experiments, *J. Am. Chem. Soc. 108*, 4285−4294.
28. Patt, S. L., and Sykes, B. D. (1972) Water Eliminated Fourier Transform NMR Spectroscopy, *J. Chem. Phys. 56*, 3182−3184.
29. Lankhorst, P. P., Wille, G., van Boom, J. H., Altona, C., and Haasnoot, C. A. G. (1983) Conformational Analysis of a Ribopentanucleoside Tetraphosphate in Aqueous Solution. A Two-Dimensional NMR Study at 500 MHz, *Nucleic Acids Res. 11*, 2839−2856.
30. Jeneer, J., Meier, B. H., Bachmann, P., and Ernst, R. R. (1979) Investigation of exchange processes by two-dimensional NMR spectroscopy, *J. Chem. Phys. 71*, 4546−4553.
31. Kitagawa, T. (1988) in *Heme protein structure and the iron-histidine stretching mode* (Spiro, T., Ed.) pp 97−131, John Wiley & Sons, New York.
32. Ray, G. B., Li, X.-Y., Ibers, J. A., Sessler, J. L., and Spiro, T. G. (1994) How far can proteins bend the FeCO unit? Distal polar and steric effects in heme proteins and models, *J. Am. Chem. Soc. 116*, 162−176.
33. Phillips, G. N., Jr., Teodoro, M. L., Li, T., Smith, B., and Olson, J. S. (1999) Bound CO Is A Molecular Probe of Electrostatic Potential in the Distal Pocket of Myoglobin, *J. Phys. Chem. B 103*, 8817−8829.
34. Li, T., Quillin, M. L., Phillips, G. N., Jr., and Olson, J. S. (1994) Structural determinants of the stretching frequency of CO bound to myoglobin, *Biochemistry 33*, 1433−1446.
35. Liu, Y., Zhang, X., Yoshida, T., and La Mar, G. N. (2004) ^{1}H NMR characterization of the solution active site structure of substrate-bound, cyanide-inhibited heme oxygenase from *Neisseria meningitidis*: Comparison to crystal structures, *Biochemistry 43*, 10112−10126.
36. Rivera, M., and Caignan, G. A. (2004) Recent Developments in the ^{13}C NMR Spectroscopic Analysis of Paramagnetic Hemes and Heme Proteins, *Anal. Bioanal. Chem. 378*, 1464−1483.
37. Shokhirev, N. V., and Walker, F. A. (1998) The effect of axial ligand plane orientation on the contact and pseudocontact shifts of low-spin ferriheme proteins, *J. Biol. Inorg. Chem. 3*, 581−594.

BI050810T